atmosphere

MDPI

Article

Impact of Fake Below-Ground Meridional Wind on Hadley Circulation: Climatology, Interannual Variability, and Long-Term Trends

Jianbo Cheng [1,2], Zhihang Xu [2,*] and Xiaoya Hou [2]

[1] School of Environmental Science and Engineering, Yancheng Institute of Technology, Yancheng 224051, China; chengjb10@lzu.edu.cn

[2] Key Laboratory of Semi-Arid Climate Change of Ministry of Education, College of Atmospheric Sciences, Lanzhou University, Lanzhou 730000, China; houxy2013@lzu.edu.cn

* Correspondence: xuzhh17@lzu.edu.cn

Received: 8 April 2020; Accepted: 26 April 2020; Published: 29 April 2020

Abstract: The fake below-ground meridional wind (FBGMW) exists in reanalysis products which is not present in the real atmosphere and should be removed before calculating the mass stream function (MSF). In this study, the impacts of FBGMW on Hadley circulation (HC) in terms of climatology, interannual variability, and long-term trends were investigated using five reanalysis data sets based on three different computing methods. Generally, the impacts of FBGMW on the HC are most notable, although the absolute magnitude of the FBGMW is rather small. The key finding of this study is that the FBGMW has vital influences on the Northern Hemisphere (NH) HC during boreal summer. This is because the NH HC during boreal summer is very weak; the errors of the MSF caused by not considering FBGMW have more obvious influences on the NH HC during boreal summer than that in other months. The previous analysis without considering FBGMW led to overestimation of the poleward expansion of the NH HC during boreal summer, and the long-term trends of the HC should be more accurately estimated after considering the FBGMW. This finding suggests that the previous studies related to the NH HC during boreal summer without considering FBGMW should be reconsidered.

Keywords: fake below-ground meridional wind; Hadley circulation; impact; climatology; interannual variability; long-term trends

1. Introduction

The differential solar heating of Earth's surface between the tropics and extratropics results in Hadley circulation (HC) which is characterized by warm air rising over equatorial areas and cool air sinking over the subtropics in both hemispheres [1,2]. Hadley circulation is one of the fundamental members of the monsoon system and is closely related to the wind belt, westerly jet, large-scale vortex, and through. In addition, HC plays an important role in the transport and exchange of energy, mass, angular momentum, water vapor, and other variables between low and middle–high latitudes. Thus, HC is crucially important to the mean state and variability of global weather and climate systems [3–5].

Motivated by the vital importance of HC, there has been growing interest in studying the intensity and width of HC over the past few years. Various studies claimed that HC has strengthened in recent decades [6–11]. For example, Chen et al. [6] and Wielicki et al. [11] suggested an increase in the outgoing longwave radiation (OLR) in subtropical areas, demonstrating a strengthening of the tropical overturning circulations, particularly HC. Sohn and Park [8] also found an intensification of HC from the perspective of water vapor transport. Specifically, several widely used reanalysis data sets and observations have shown an obvious strengthening trend of the boreal winter HC [4,7,12,13], while

minor changes have been found in the boreal summer HC in recent years [14,15]. The long-term changes of the regional HC have also been investigated in previous studies [10,16,17]. For example, Chen et al. [10] investigated changes in the strength of the regional annual mean HC over six different regions and found that these six regional HCs have generally strengthened in both hemispheres. Freitas et al. [16] studied the HC intensity changes in the Indian Ocean region and found that it has vital influences on surrounding regions. Huang et al. [17] suggested that the spring HC has strengthened in both hemispheres, and this finding can be obtained in various different re-analyses.

Since the subtropical dry zones are closely connected with the sinking branch of HC, meridional shifts of the sinking branch can lead to changes in precipitation and temperature patterns; thus, any changes in the meridional width of HC can have vital influences on natural ecosystems, agriculture, and water resources. Numerous theoretical and modeling studies based on different metrics have demonstrated that HC has expanded poleward in recent decades, implying a poleward expansion of the subtropical dry zones [18]. These metrics include the meridional mass stream function (MSF) [9,19–21], tropical tropopause heights [22,23], stratospheric ozone [5,24], OLR [19,25], subtropical jet streams [26], sea-level pressure [25], and precipitation [25,27,28]. Although these metrics displayed the different magnitudes and seasonality of the trends, they all suggested systematic and significant expansion of the HC [18].

The meridional wind in some reanalysis data sets and model outputs exists from 1000 hPa to the top of the atmosphere. However, there exist topography and seas around the world, and the surface pressure in some regions is lower than 1000 hPa; thus, meridional wind in those regions in the lower troposphere is actually nonexistent, and it is defined as the fake below-ground meridional wind (hereafter FBGMW) in this study. In a recent study, Cheng et al. [29] proposed that FBGMW has a vital influence on HC when the MSF is used to investigate HC. Specifically, the MSF is commonly calculated from the meridional wind as follows [3]:

$$\psi = \frac{2\pi a \cos\varphi}{g} \int_{p_s}^{p} [v] dp, \tag{1}$$

where a is the Earth's radius, φ is the latitude, g is the gravitational acceleration, p is the pressure, p_s is the surface pressure, v is the meridional wind, and square brackets indicate the zonal mean. If we assume that the surface pressure p_s equals 1000 hPa, then the FBGMW can cause errors when calculating the MSF through Equation (1). Figure 1 displays the Northern Hemisphere (NH) HC between 10° N and 50° N in July 1979 represented by the MSF without and with considering FBGMW, and the difference between them. Cheng et al. [29] claimed that based on the MSF that does not consider FBGMW (i.e., p_s equals 1000 hPa), a "minor circulation" characterized as southward circulation embedded within the conventional northward circulation is evident in the NH HC during boreal summer (Figure 1a). However, after considering FBGMW (i.e., the real p_s is used), the NH HC is characterized as a single northward circulation at low latitudes (Figure 1d). In other words, the FBGMW can lead to considerable biases in the NH HC by the process of vertical integration (Figure 1g). Since the positive structure of the difference is more evident than the HC that considers FBGMW in the mid–high latitudes (compare Figure 1d,g), the difference leads to the splitting of the boreal summer HC peaking at 20°–25° N and 35° N, i.e., the difference results in the second cell which has a peak at approximately 35° N (Figure 1a). Cheng et al. [29] also pointed out that not considering FBGMW could lead to a miscalculation of the location of the sinking branch of HC in some years (compare the location where the red and blue lines cross zero in Figure 1j). In addition, the results derived from three different methods (i.e., the traditional method (hereafter M1) proposed by Oort and Yienger [3], the local partitioning method (hereafter M2) proposed by Schwendike et al. [30,31], and the three-pattern decomposition of global atmospheric circulation (3P-DGAC) method (hereafter M3) proposed by Hu et al. [32–34]) were quite similar (Figure 1).

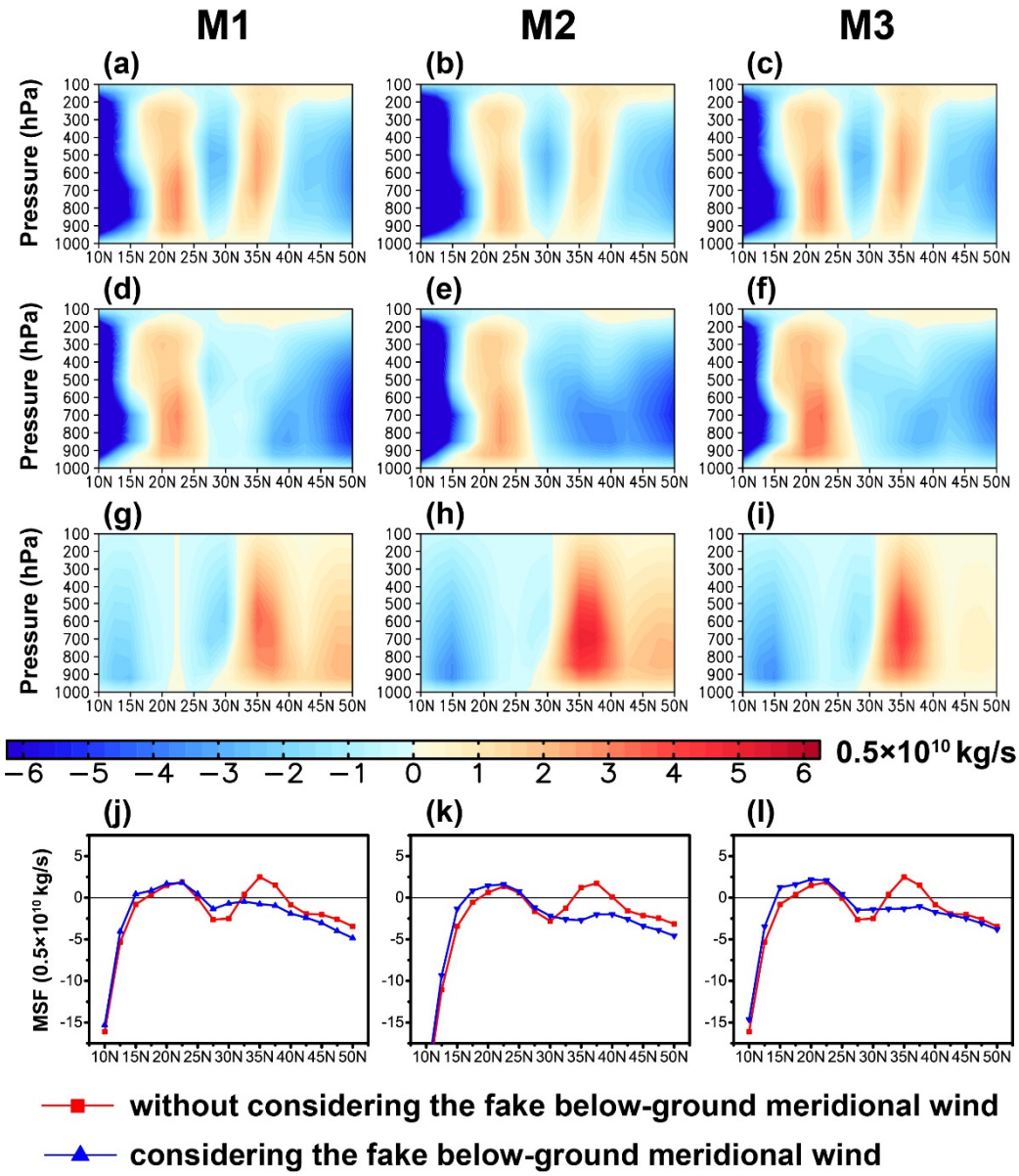

Figure 1. (**a**–**c**) Northern Hemisphere (NH) Hadley circulation (HC) between 10° N and 50° N in July 1979 represented by the mass stream function (MSF) derived from the (**a**) traditional method (M1), (**b**) local partitioning method (M2), and (**c**) three-pattern decomposition of global atmospheric circulation (3P-DGAC, M3) without considering fake below-ground meridional wind (FBGMW) using the National Centers for Environmental Prediction (NCEP)/Department of Energy (DOE) Reanalysis (hereafter NCEP2) data sets. (**d**–**f**) Same as (**a**–**c**) but for the NH HC represented by the MSF that considers FBGMW. (**g**–**i**) Same as (**a**–**c**) but for the difference between the uncorrected and corrected NH HC. (**j**–**l**) Latitudinal distribution of the MSF between 10° N and 50° N at 500 hPa in July 1979 derived from (**j**) M1, (**k**) M2, and (**l**) M3. The red and blue lines represent the latitudinal distribution of the MSF without and with considering FBGMW, respectively. The units for the MSF are 0.5×10^{10} kg/s.

Generally, a previous study showed that FBGMW has a vital influence on the NH HC during boreal summer. However, FBGMW exists throughout the year in both hemispheres, and Cheng et al. [29] focused only on the NH HC during boreal summer; thus, the impact of FBGMW on HC in all months and hemispheres should be further investigated. In this study, we aimed to investigate the impact of FBGMW on HC in terms of climatology, interannual variability, and long-term trends, and the following two main concerns were investigated:

(1) Does FBGMW have an impact on HC in all months and hemispheres?

(2) According to previous studies [32–34], the three computing methods (i.e., M1, M2, and M3) are not identical. What are the features of the impact of FBGMW on HC based on the three methods?

The remainder of this paper is organized as follows. The data sets and metrics used in this study are described in the next section. The impacts of FBGMW on the climatology, interannual variability, and long-term trends of HC are examined in Section 3. Finally, we provide conclusions and discussion in Section 4.

2. Data and Methods

2.1. Data

To avoid data dependence on the main conclusions obtained in this study, we employed the monthly horizontal winds and surface pressure derived from five different reanalysis data sets: the Climate Forecast System Reanalysis (CFSR) and CFSR Version 2 (hereafter CSFR) [35,36], the European Centre for Medium-Range Weather Forecast (ECMWF) Interim Reanalysis (hereafter ERA-Interim) [37], the fifth generation of ECMWF atmospheric re-analyses of the global climate (hereafter ERA5) [38], the Japanese Meteorological Agency 55 year Reanalysis (hereafter JRA-55) [39], and the National Centers for Environmental Prediction (NCEP)/Department of Energy (DOE) Reanalysis (hereafter NCEP2) [40]. To be consistent with each other, all data sets used in this study were interpolated to a common 2.5° × 2.5° horizontal grid, and the 17 most commonly used pressure levels (i.e., 1000, 925, 850, 700, 600, 500, 400, 300, 250, 200, 150, 100, 70, 50, 30, 20, and 10 hPa) were chosen. The analyzed time period in this study was from 1979 to 2018.

2.2. Three Methods for Calculating the MSF

To answer the questions proposed in Section 1, the three methods for calculating the MSF of HC (i.e., the traditional method (M1) proposed by Oort and Yienger [3], the local partitioning method (M2) proposed by Schwendike et al. [30,31], and the 3P-DGAC method (M3) proposed by Hu et al. [32–34]) were adopted in this study. Descriptions and a theoretical comparison among the three methods can be obtained in Hu et al. [32], Cheng et al. [29], and also in the Supplementary Materials of this study. The analyses was based on the MSF derived from the M1 (ψ_1), M2 (ψ_2), and M3 (ψ_3) as follows:

$$\begin{cases} \psi_1 = \frac{2\pi a \cos\varphi}{g} \int_{p_s}^{p} [v] dp, \\ \psi_2 = \frac{2\pi a \cos\varphi}{g} \int_{p_s}^{p} [v_{div}] dp, \\ \psi_3 = \frac{2\pi a \cos\varphi}{g} \int_{p_s}^{p} [v_H] dp, \end{cases} \quad (2)$$

where v, v_{div}, and v_H are the meridional winds of HC based on M1, M2, and M3, respectively. Specifically, v is the original meridional wind, v_{div} is the divergence meridional wind, and v_H is the meridional wind of the Meridional circulation defined by Hu et al. [32–34]. It should be noted that the global zonally averaged meridional winds derived from the three methods are almost identical (i.e., $[v] = [v_{div}] = [v_H]$) when the FBGMW is not removed from the re-analyses. After removing the FBGMW from the re-analyses, the global zonally averaged meridional wind derived from the three methods are different, i.e., $[v] \neq [v_{div}] \neq [v_H]$ [29,32]. As proposed in Section 1, if we assume the surface pressure, p_s, equals 1000 hPa, then FBGMW can cause errors when calculating the MSF through Equation (2). On the other hand, the errors caused by FBGMW can be solved by using the real surface pressure. Hence, the impact of FBGMW on HC can be investigated by comparing the two cases proposed above by using different p_s values.

2.3. Definition of the Intensity, Rising, and Sinking Branches and Width of HC

According to previous studies [3], the NH (Southern Hemisphere (SH)) HC intensity (HCI) is defined as the maximum (minimum) value of the MSF in the latitudinal band of 0°–30° N (0°–30° S)

between 925 and 200 hPa; thus, the NH (SH) HCI is positive (negative). It should be mentioned that if the HCI is defined as the maximum (minimum) value of the vertically averaged MSF between 925 and 200 hPa or defined as the vertically averaged value of the maximum (minimum) value of the MSF at each pressure level from 925 to 200 hPa, the main conclusions obtained in this study will not change.

The position of the rising branch of HC (i.e., the common inner edge (CE) separating the NH and SH HC) is defined as the latitude where the MSF at 500 hPa changes sign at low latitudes. The position of the sinking branch of HC (i.e., the northern edge (NE) or southern edge (SE) of the HC) is defined as the latitude where the MSF at 500 hPa transits from HC to Ferrel circulation (i.e., where the MSF at 500 hPa equals zero in subtropical areas) in each hemisphere. Thus, a positive (negative) value represents that the rising or sinking branch is located in the NH (SH). The width of the HC (hereafter HCW) in each hemisphere is defined as the difference between the HC poleward edges (NE and SE) and CE, and the total width of the HC (hereafter TOT HCW) is defined as the difference between NE and SE. Thus, the NH and TOT (SH) HCWs are both positive (negative). It should be mentioned that if the definitions of the CE, NE, and SE are based on the vertically averaged MSF between 925 and 200 hPa or between 700 and 300 hPa or between 600 and 400 hPa, the main conclusions obtained in this study will not change. The acronyms used in this study are listed in Table 1.

Table 1. List of the acronyms used in this study.

List	Acronyms
Hadley circulation	HC
Mass stream function	MSF
Fake below-ground meridional wind	FBGMW
Northern Hemisphere	NH
Southern Hemisphere	SH
HC intensity	HCI
Common inner edge	CE
Northern edge	NE
Southern edge	SE
HC width	HCW
Total HC width	TOT HCW
Multi-re-analyses mean	MRM

3. Impact of the Fake Below-Ground Meridional Wind on HC

3.1. Climatology

Figure 2 displays the global distribution of the mean state of the surface pressure from the multi-re-analysis mean (MRM) during 1979–2018. Figure 2 shows that the global distributions of the surface pressure from different months are quite similar, and the surface pressure over most land and Antarctic regions is less than 1000 hPa, suggesting that the impact of FBGMW on HC exists in all months.

Figures 3–5 display the mean state of the uncorrected (i.e., p_s equals 1000 hPa) and corrected (i.e., the real p_s is used) HC and the difference between them derived from three calculation methods. Figures 3–5 show that FBGMW had an influence on the mean state of the HC in all months and hemispheres, and the errors caused by not considering FBGMW derived from M1, M2, and M3 were different. By comparing the mean state of the HC (black contours) and the difference (i.e., error) caused by not considering FBGMW (shading) in Figures 3–5, it was found that the error and mean state of the NH HC had the same magnitude during boreal summer, while the error was much smaller than the mean state in other seasons and in the SH. Thus, not considering FBGMW has a vital influence on the spatial pattern of the NH HC during boreal summer (e.g., Figure 1). In other seasons and in the SH, the spatial patterns of the mean state of the uncorrected and corrected HC were similar (figure not shown). Namely, although errors exist in all months and hemispheres, only the spatial pattern

of the NH HC during boreal summer was greatly influenced. In addition, the differences caused by not considering FBGMW derived from the three calculation methods were similar in the NH during boreal summer which were all characterized as anomalous southward (northward) circulation at low (middle) latitudes in the NH (Figure 3f–h, Figure 4f–h, and Figure 5f–h), leading to the similar "minor circulation" structure of the uncorrected NH HC obtained from the three methods as shown in Figure 1.

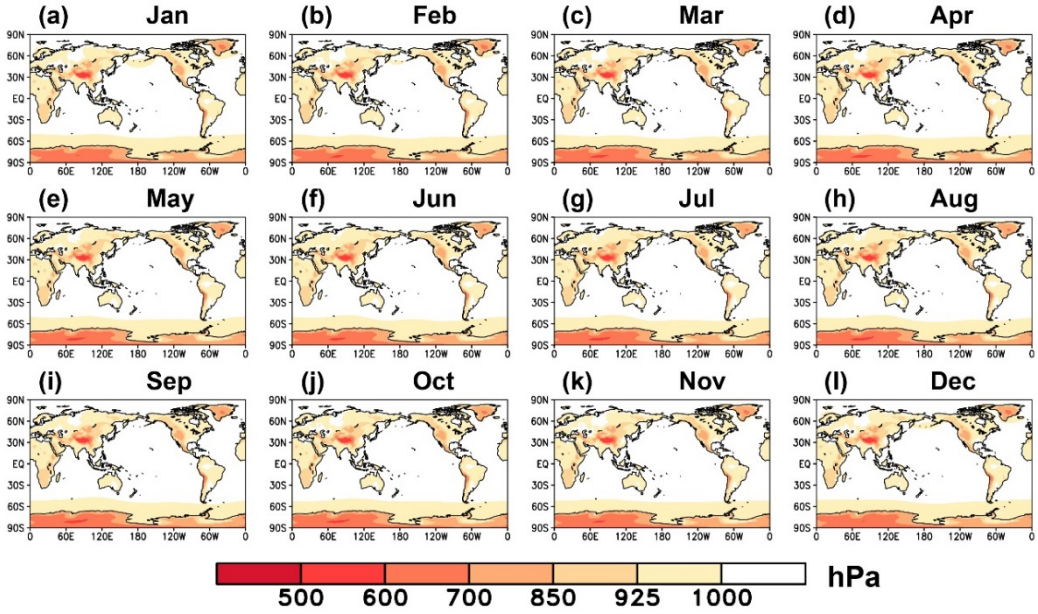

Figure 2. Global distribution of the mean state of the surface pressure from the MRM during 1979–2018. (**a**–**l**) The surface pressure from January to December. The units for the surface pressure are hPa.

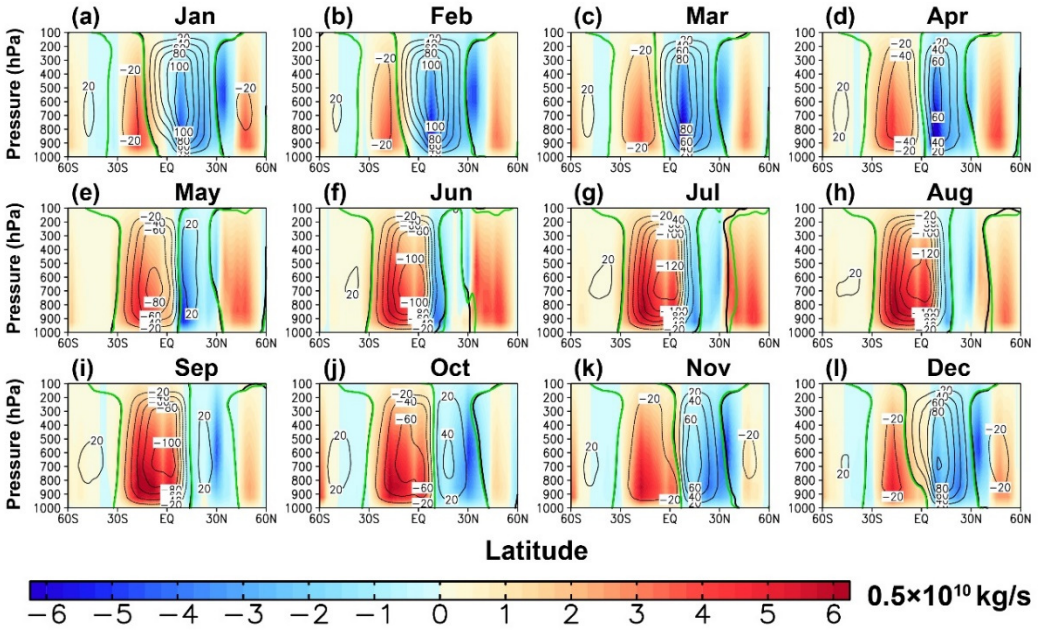

Figure 3. Black contours: mean state (1979–2018) of the HC between 60° S and 60° N represented by the MSF that considers FBGMW derived from M1 using the MRM data sets. Shading: difference between the uncorrected and corrected mean state of the HC. Green contours: same as black contours but for the zero lines of the MSF without considering FBGMW. (**a**–**l**) The results from January to December. The units for the MSF are 0.5×10^{10} kg/s.

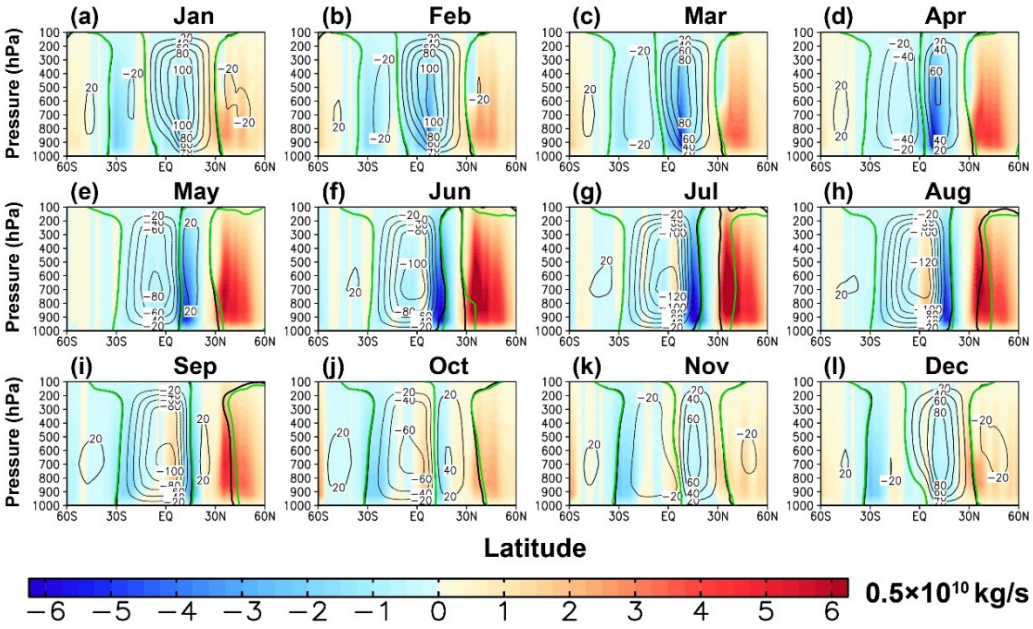

Figure 4. Same as Figure 3 but for the results derived from M2.

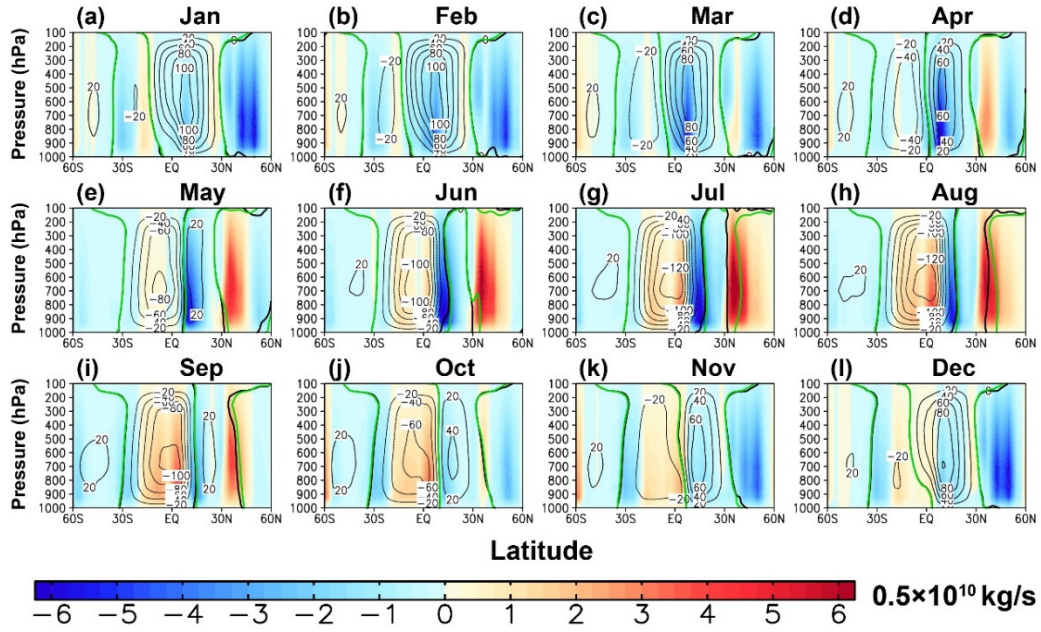

Figure 5. Same as Figure 3 but for the results derived from M3.

Figure 6 displays the annual cycle of the intensity, rising and sinking branches, and width of the uncorrected and corrected HC derived from M1, M2, and M3 using the MRM data sets from 1979–2018. Figure 7 displays the annual cycle of the difference between the uncorrected and corrected HC intensity, rising and sinking branches, and width derived from M1, M2, and M3 using the MRM data sets from 1979–2018. In terms of the HCI, Figure 6a, and Figure 7a,d show that based on M1 and not considering FBGMW led to underestimation of the HCI in all months and hemispheres, and the underestimation of the NH HCI in June to September was relatively small. However, Figures 6 and 7 show that the results based on M2 and M3 were different from those derived from M1, especially in the SH. Based on M2 and not considering FBGMW led to underestimation of the NH HCI from January to June and had a small impact on the NH HCI in other months and on the SH HCI in all months. Based on M3 and not considering FBGMW led to underestimation of the NH (SH) HCI from January to July and October

to December (July to December) and had a small impact on the HCI in other months. Although the absolute difference between the uncorrected and corrected HCI in some months was small, the relative difference was large in these months, suggesting that the error caused by not considering FBGMW still had a vital influence on the HC in these months regardless of the small absolute value (Figure 7). For example, Figure 7a,g (Figure 7d,j) show that although the absolute difference between the uncorrected and corrected NH (SH) HCI based on M1 in July (January to March) was small, the relative difference was much larger than that in many other months, suggesting that the error caused by not considering FBGMW had a vital influence on the NH (SH) HCI in July (January to March). A similar phenomenon can be obtained from M2 and M3.

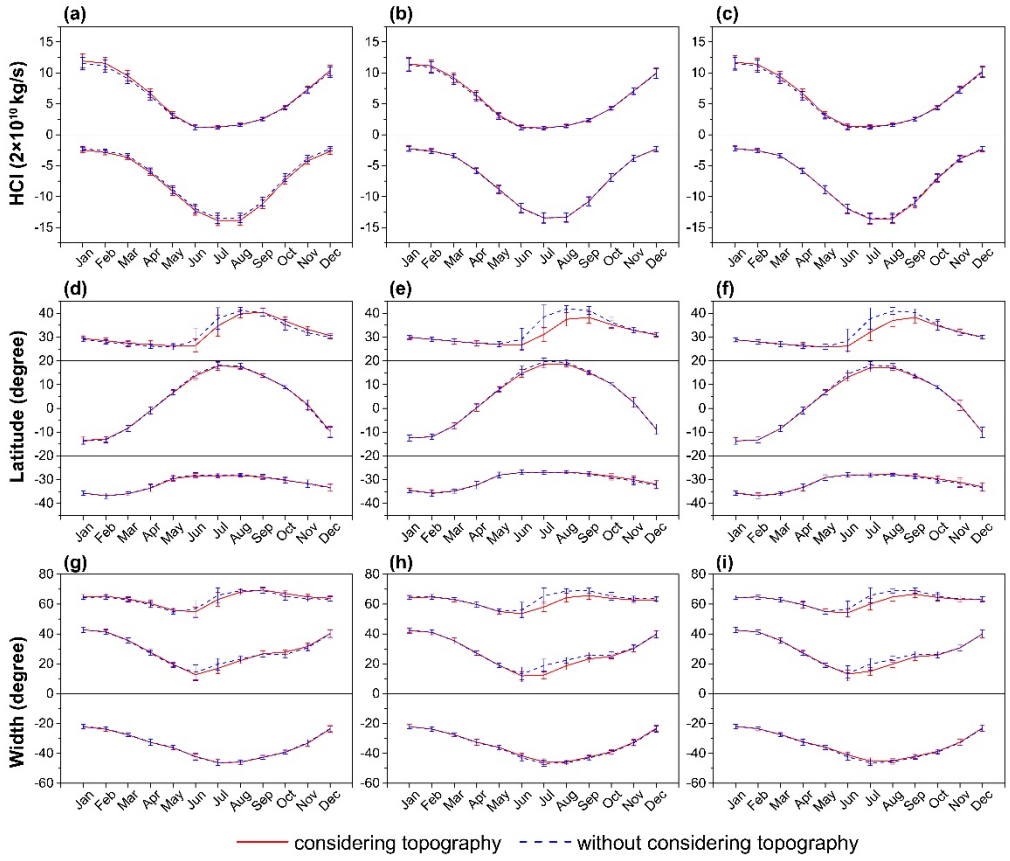

Figure 6. (**a**–**c**) Annual cycle of the NH (upper) and SH (lower) HCI derived from (**a**) M1, (**b**) M2, and (**c**) M3 using the MRM data sets from 1979–2018. The red, solid line and blue, dashed line represent the annual cycle of the HCI without and with considering FBGMW, respectively. (**d**–**f**) Same as (**a**–**c**) but for the annual cycle of the NE (upper), CE (middle), and SE (lower). (**g**–**i**) Same as (**a**–**c**) but for the annual cycle of the TOT (upper), NH (middle), and SH (lower) HCW. The vertical bars in each plot represent the standard deviation of the interannual variability. The units for the HCI are 2×10^{10} kg/s, and the units for the NE, CE, SE, TOT HCW, NH HCW, and SH HCW are degrees.

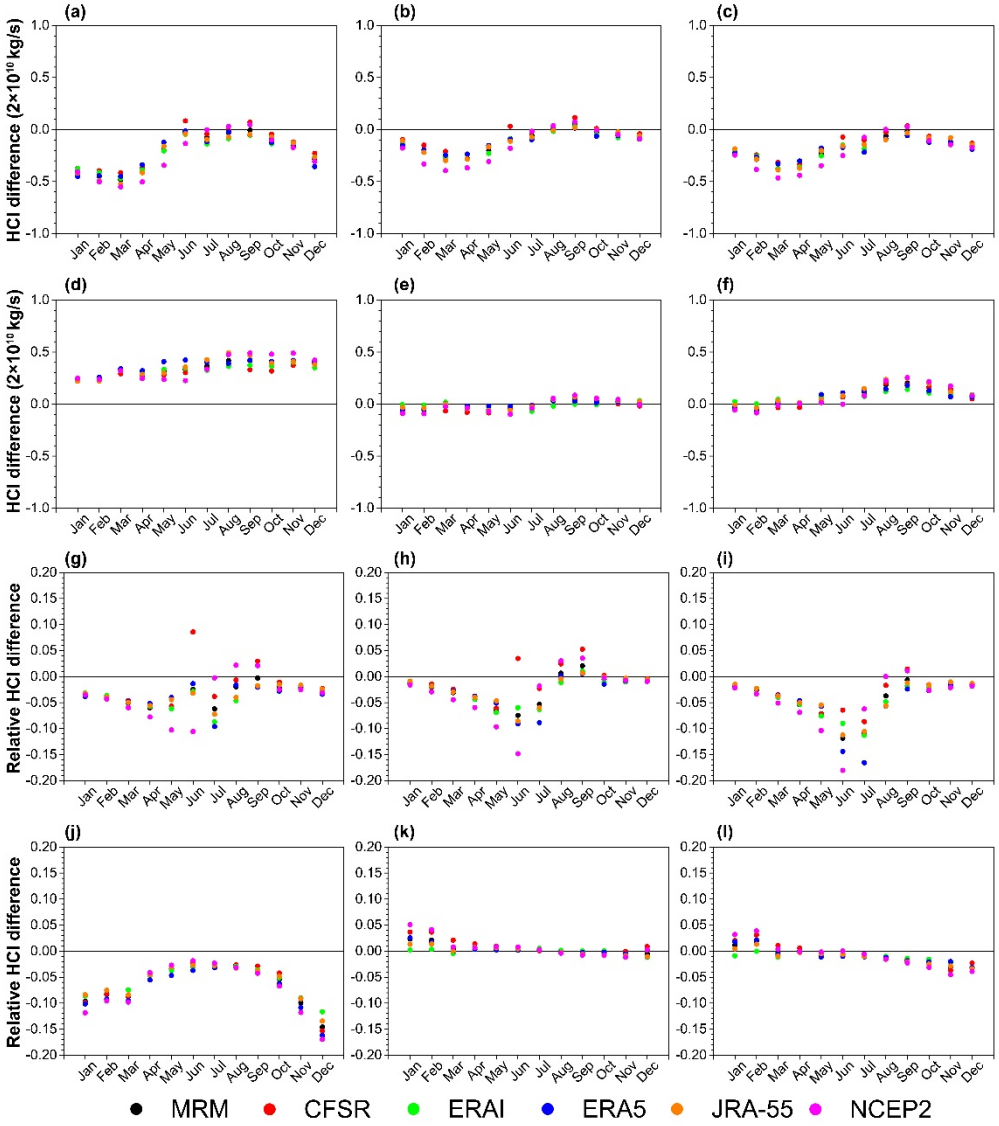

Figure 7. (**a**–**c**) Annual cycle of the difference between the uncorrected and corrected NH HCI derived from (**a**) M1, (**b**) M2, and (**c**) M3 using the MRM (black), the Climate Forecast System Reanalysis (CFSR) and CFSR Version 2 (hereafter CSFR; red), the European Centre for Medium-Range Weather Forecast (ECMWF) Interim Reanalysis (hereafter ERA-Interim; green), the fifth generation of ECMWF atmospheric re-analyses of the global climate (hereafter ERA5; blue), the Japanese Meteorological Agency 55 year Reanalysis (hereafter JRA-55; orange), and NCEP2 (magenta) data sets from 1979–2018. (**d**–**f**) Same as (**a**–**c**) but for the annual cycle of the difference between the uncorrected and corrected SH HCI. (**g**–**i**) Same as (**a**–**c**) but for the annual cycle of the relative difference between the uncorrected and corrected NH HCI (i.e., the difference divided by the mean value of the corrected NH HCI). (**j**–**l**) Same as (**g**–**i**) but for the annual cycle of the relative difference between the uncorrected and corrected SH HCI. The units for the HCI difference are 2×10^{10} kg/s.

The comparison of the red and blue lines in Figure 6d shows that based on M1 and not considering FBGMW led to an obvious poleward shift of the NE from June to August and an equatorward shift of the NE in other months, while it led to small changes in the SE in all months (see also Figure 8). In addition, not considering FBGMW led to a poleward shift of the CE from June to August and small changes in the CE in other months. Figures 6 and 8 show that the results obtained from M2 and M3 were similar to those obtained from M1 for the SE and CE. The results obtained from M2 and

M3 suggest that not considering FBGMW led to an obvious poleward shift of the NE from June to September and small changes in the NE in other months which is different from that obtained from M1.

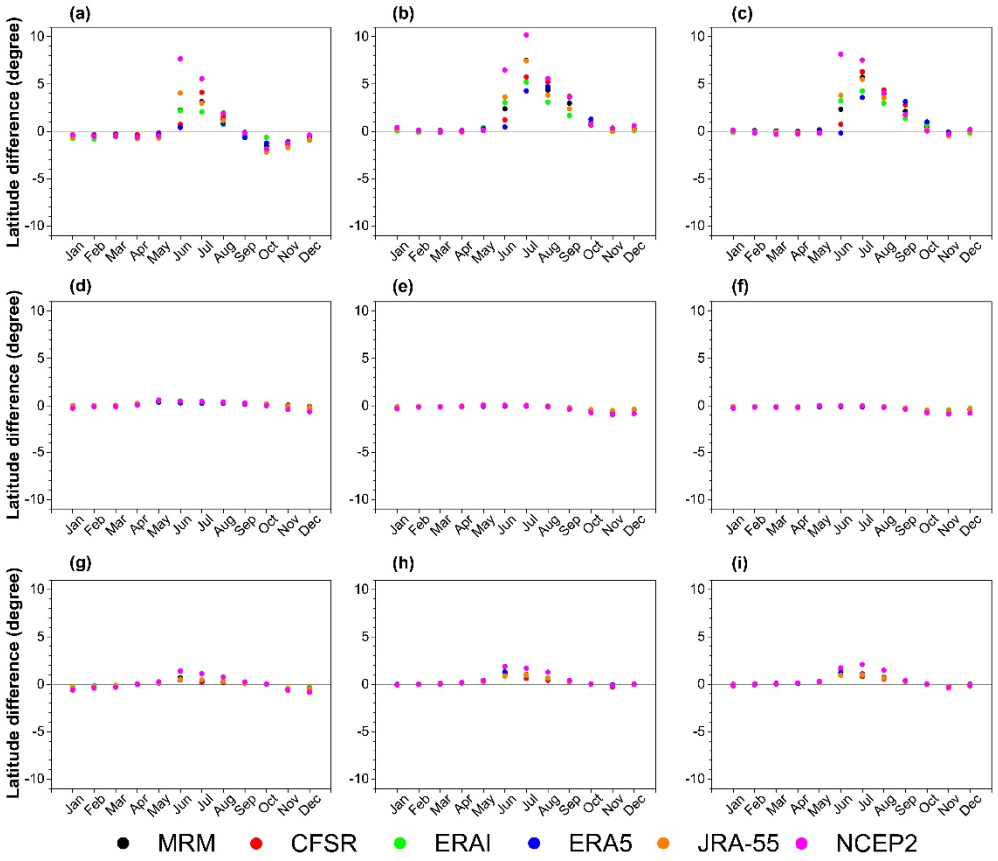

Figure 8. (**a**–**c**) Annual cycle of the difference between the uncorrected and corrected NE derived from (**a**) M1, (**b**) M2, and (**c**) M3 using the MRM (black), CFSR (red), ERA-Interim (green), ERA5 (blue), JRA-55 (orange), and NCEP2 (magenta) data sets from 1979–2018. (**d**–**f**) and (**g**–**l**) are the same as (**a**–**c**) but for the SE and CE, respectively. The units for the NE, CE, and SE difference are degrees.

Since the HCW is defined by using the NE, SE, and CE, not considering FBGMW also led to errors in the HCW. Because the error in the NE was much larger than that in the CE during boreal summer, and the errors in the NE and CE were both small in other months, the error in the NH HCW was similar to that in the NE (Figures 8a–c and 9a–c). Similarly, because the error in the SE caused by not considering FBGMW was much smaller than that in the NE during boreal summer, and the errors in the NE and SE were both small in other months, the error in the TOT HCW was also similar to that in the NE (Figures 8a–c and 9g–i). In addition, because not considering FBGMW led to a poleward shift of the CE from June to August and to small changes in the SE, the error led to the contraction of the SH HCW from June to August. In other months, the error in the SH HCW was small.

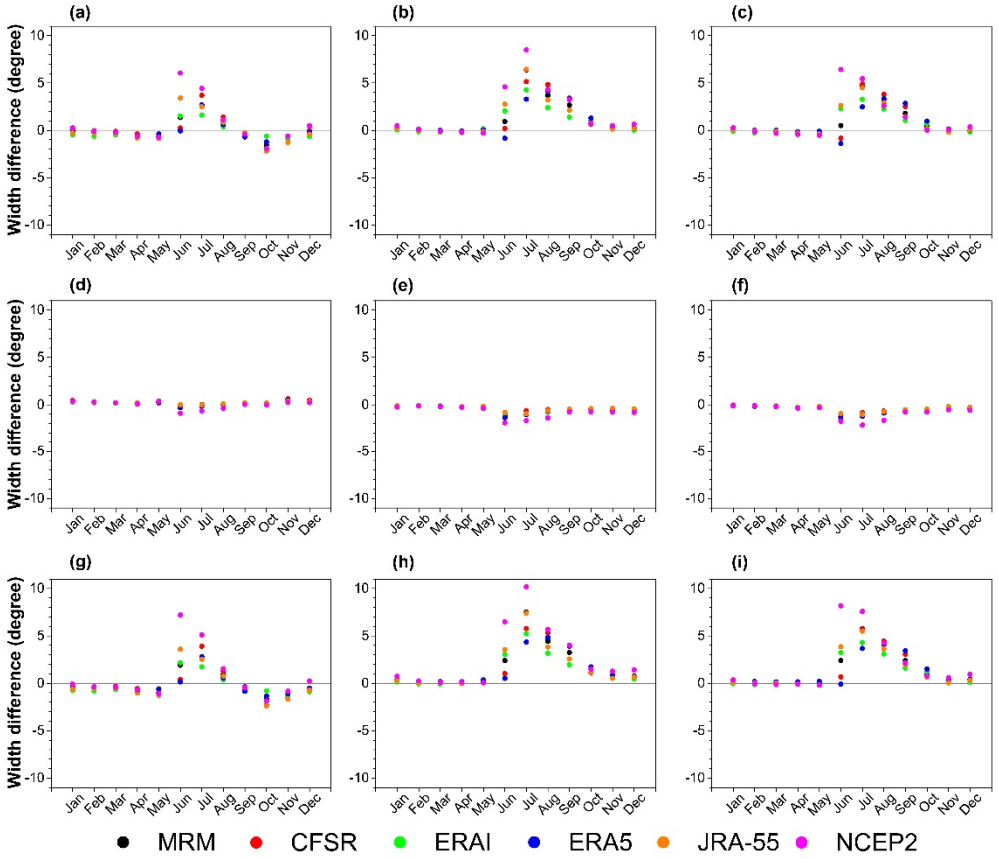

Figure 9. (**a**–**c**) Annual cycle of the difference between the uncorrected and corrected NH HCW derived from (**a**) M1, (**b**) M2, and (**c**) M3 using the MRM (black), CFSR (red), ERA-Interim (green), ERA5 (blue), JRA-55 (orange), and NCEP2 (magenta) data sets from 1979–2018. (**d**–**f**) and (**g**–**i**) Same as (**a**–**c**), but for the SH and TOT HCW, respectively. The units for the NH, SH, and TOT HCW difference are degrees.

3.2. Interannual Variability

Figure 10 displays the correlation between the uncorrected and corrected HCI, rising and sinking branches, and width derived from M1, M2, and M3 from 1979–2018. The results shown in Figure 10 derived from different methods and reanalysis data sets were similar, implying that the impacts of FBGMW on the interannual variability in HC were similar based on different methods regardless of the reanalysis data set. Figure 10a shows that the correlation between the uncorrected and corrected NH HCI was close to one from January to May and September to December, and the correlation was slightly weaker in other months. In the SH, the correlation between the uncorrected and corrected HCI was close to one in all months (Figure 10b). Thus, FBGMW had nearly no impact on the interannual variability of the NH HCI from January to May and September to December and the SH HCI in all months, while it had a small impact on the NH HCI from June to August. Figure 10c,d show that FBGMW had an impact on the interannual variability of the NE in all months, especially from June to September, while it had nearly no impact on the SE. Similar to the NH HCI, FBGMW had nearly no impact on the interannual variability of the CE from January to May and September to December, while it had a small impact on the CE from June to August (Figure 10e). As the NH (TOT) HCW is defined by using the NE and CE (SE), FBGMW had an impact on the interannual variability of the NH (TOT) HCW in all months, especially from June to September (Figure 10f,h). As the SH HCW is defined by using the SE and CE, FBGMW had a small impact on the interannual variability of the SH HCW from June to August (Figure 10g).

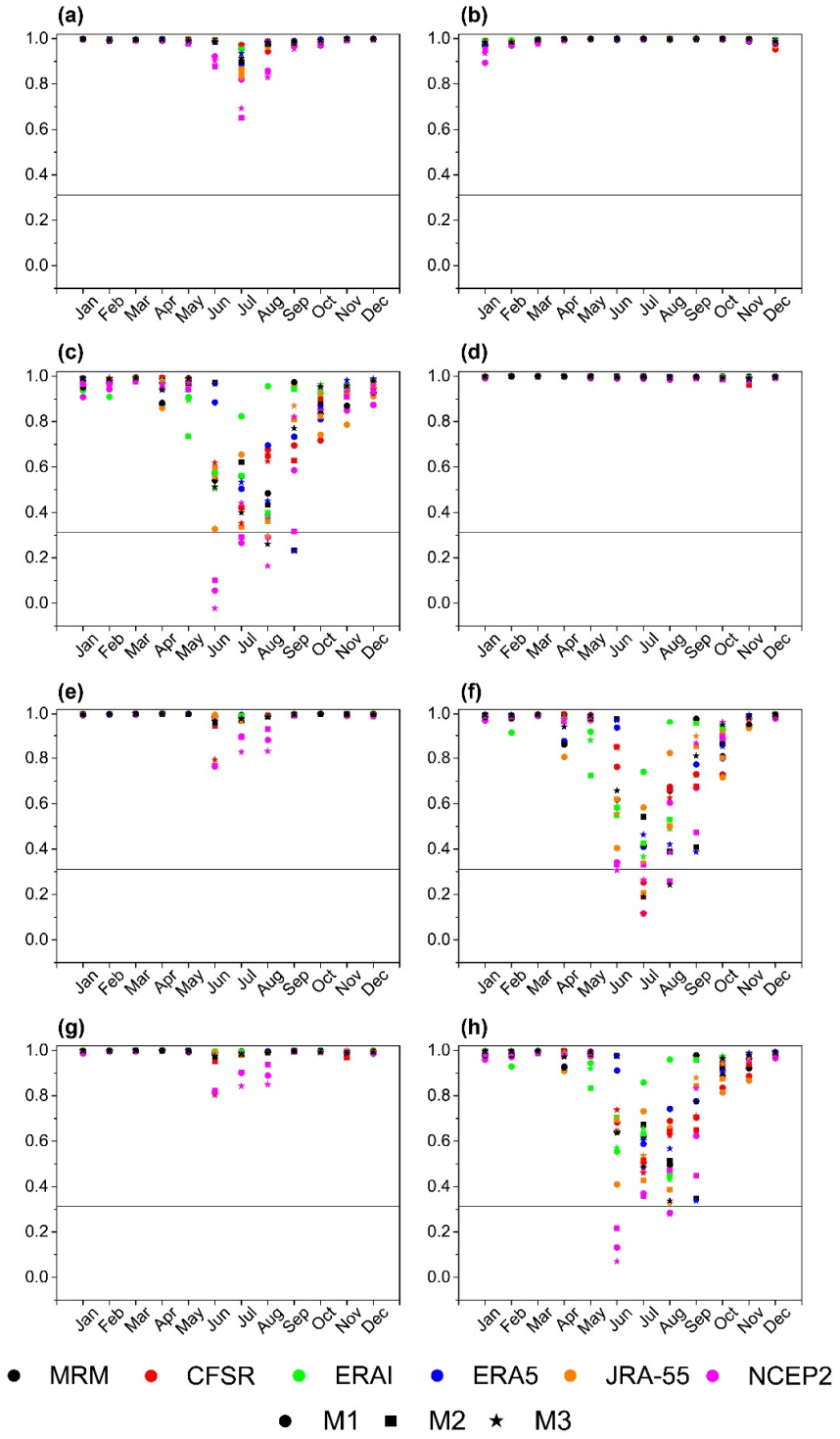

Figure 10. (**a**) Annual cycle of the correlation between the uncorrected and corrected NH HCI derived from M1 (cycle), M2 (square), and M3 (pentagram) using the MRM (black), CFSR (red), ERA-Interim (green), ERA5 (blue), JRA-55 (orange), and NCEP2 (magenta) data sets from 1979–2018. (**b**–**h**) Same as (**a**) but for the SH HCI, NE, SE, CE, NH HCW, SH HCW, and TOT HCW, respectively.

Figure 11 displays the standard deviation ratio between the uncorrected and corrected HCI, rising and sinking branches, and width derived from M1, M2, and M3 from 1979–2018. The main conclusions obtained from the correlation maps can also be found from the standard deviation ratio maps. Specifically, the impacts of FBGMW on the standard deviation of HC were similar based on

the three methods. The FBGMW had a small impact on the NH HCI, CE, and SH HCW and had an obvious impact on the NE, NH HCW, and TOT HCW from June to August, while it had nearly no impact on HC under other conditions.

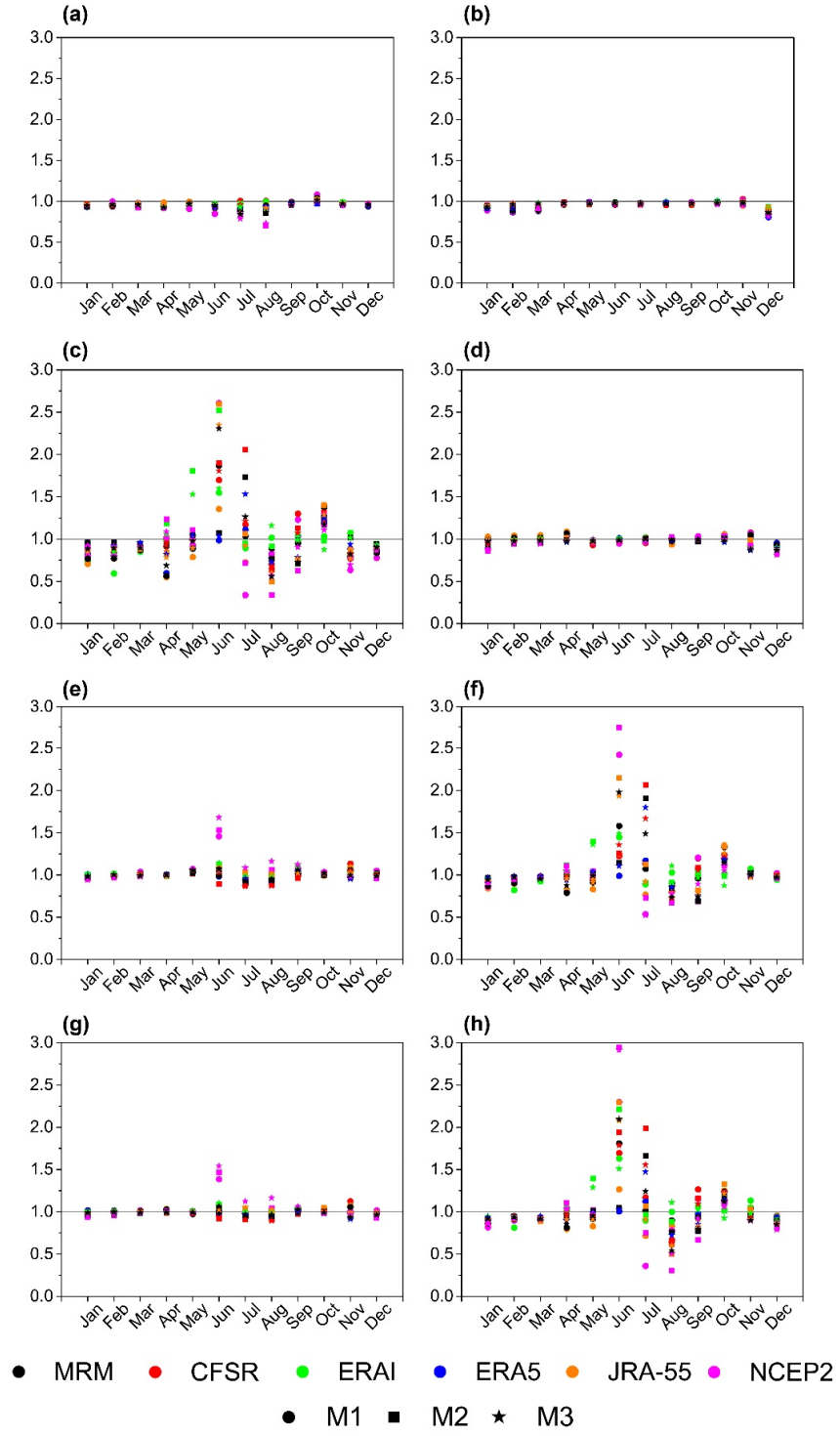

Figure 11. (**a**) Annual cycle of the standard deviation ratio between the uncorrected and corrected NH HCI derived from M1 (cycle), M2 (square), and M3 (pentagram) using the MRM (black), CFSR (red), ERA-Interim (green), ERA5 (blue), JRA-55 (orange), and NCEP2 (magenta) data sets from 1979–2018. (**b**–**h**) Same as (**a**) but for the SH HCI, NE, SE, CE, NH HCW, SH HCW, and TOT HCW, respectively.

3.3. Long-Term Trends

In this section, we do not focus on the trend itself but on the impact of FBGMW on the long-term HC trends instead. Figure 12 displays the linear trends of the HCI derived from M1 (left column), M2 (middle column), and M3 (right column) from 1979–2018 using the MRM data sets. The results shown in Figure 12 derived from different methods were similar, implying that the impacts of FBGMW on the long-term HC trends were similar based on different methods. The red and blue bars are for the results that considered FBGMW and did not consider FBGMW, respectively. The comparison of the red and blue bars in Figure 12 shows that in both hemispheres, the HCI trends when FBGMW was considered and not considered were almost identical, implying that FBGMW had a very small impact on the long-term trends of the HCI.

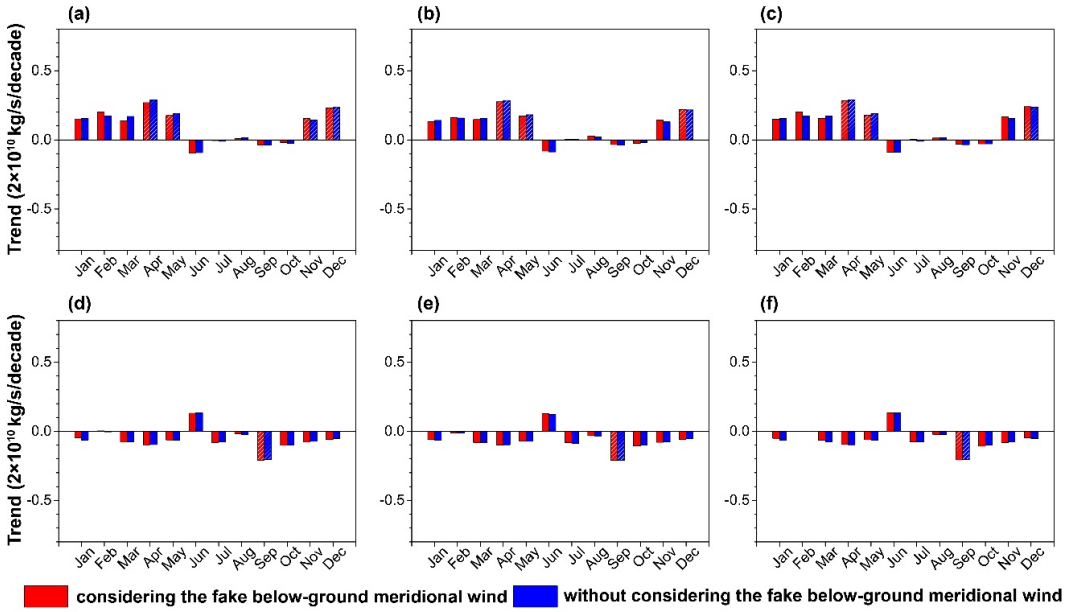

Figure 12. (**a**–**c**) Annual cycle of the linear trends of the NH HCI from 1979–2018 derived from (**a**) M1, (**b**) M2, and (**c**) M3 using the MRM data sets. The trends that passed the 95% statistical confidence level are filled with oblique lines. The red and blue bars are for the results that considered and did not consider FBGMW, respectively. (**d**–**f**) Same as (**a**–**c**) but for the SH HCI. The units for the trends are 2×10^{10} kg/s/decade.

Figure 13 displays the linear trends of the NE (upper row), SE (middle row), and CE (lower row) derived from M1 (left column), M2 (middle column), and M3 (right column) from 1979–2018 using the MRM data sets. The results obtained from the three methods all showed that FBGMW had a very small impact on the NE from January to May and October to December, while FBGMW had an obvious impact on the NE in June to September. Specifically, based on M1 and not considering FBGMW led to great poleward expansion (equatorward contraction) of the NE from June and August (July and September). Based on M2 and M3 and not considering FBGMW led to great poleward expansion of the NE from June to September. In other words, the previous analysis without considering FBGMW led to overestimation of the poleward expansion of the NH HC during boreal summer which is similar to the results of Staten et al. [41]. If FBGMW is considered, the poleward expansion of the NH HC in June was not visible. In July and September, it depends on the methods. In August, the poleward expansion of the NH HC was reduced. The results of the SE derived from different methods were similar, implying that the impacts of FBGMW on the long-term trends of the SE based on different methods were similar. The comparison of the red and blue bars in Figure 13 shows that the trends of the SE when FBGMW was considered and not considered were almost identical, implying that FBGMW had a very small impact on the long-term trends of the SE. In terms of the CE, the three

methods all showed that FBGMW had an impact on the CE in June, while FBGMW had a very small impact on the CE in other months.

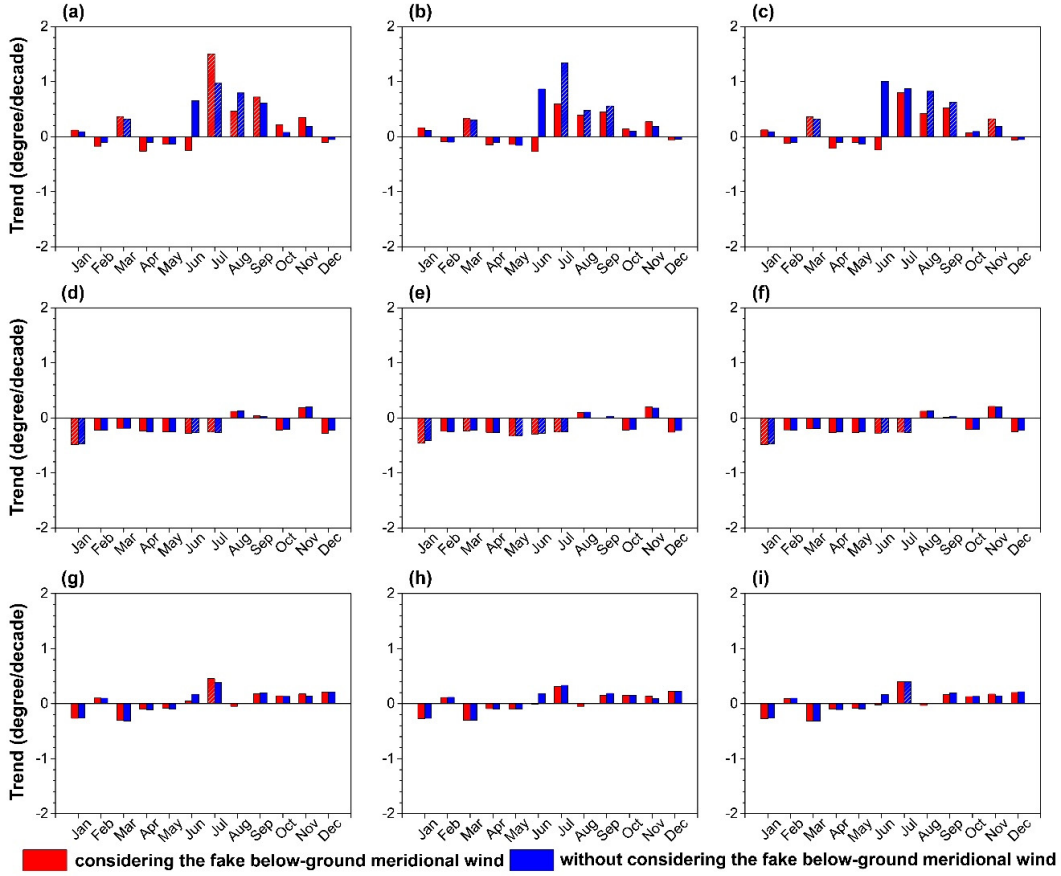

Figure 13. (**a**–**c**) Annual cycle of the linear trends of the NE from 1979–2018 derived from (**a**) M1, (**b**) M2, and (**c**) M3 using the MRM data sets. The trends that passed the 95% statistical confidence level are filled with oblique lines. The red and blue bars are for the results that considered and did not consider FBGMW, respectively. (**d**–**f**) and (**g**–**i**) same as (**a**–**c**) but for the SE and CE, respectively. The units for the trends are degree/decade.

Figure 14 displays the linear trends of the NH (upper row), SH (middle row), and TOT (lower row) HCW derived from M1 (left column), M2 (middle column), and M3 (right column) from 1979–2018 using the MRM data sets. Since the NH (TOT) HCW is defined by using the NE and CE (SE), the results of the NH (TOT) HCW were similar to those of the NE. Namely, the three methods all showed that FBGMW had a very small impact on NH (TOT) HCW from January to May and October to December, while FBGMW had an obvious impact on the NH (TOT) HCW from June to September. Since the SH HCW is defined by using the SE and CE, the results of the SH HCW were similar to those of the SE. Namely, the three methods all showed that FBGMW had an impact on SH HCW in June, while FBGMW had a very small impact on SH HCW in other months.

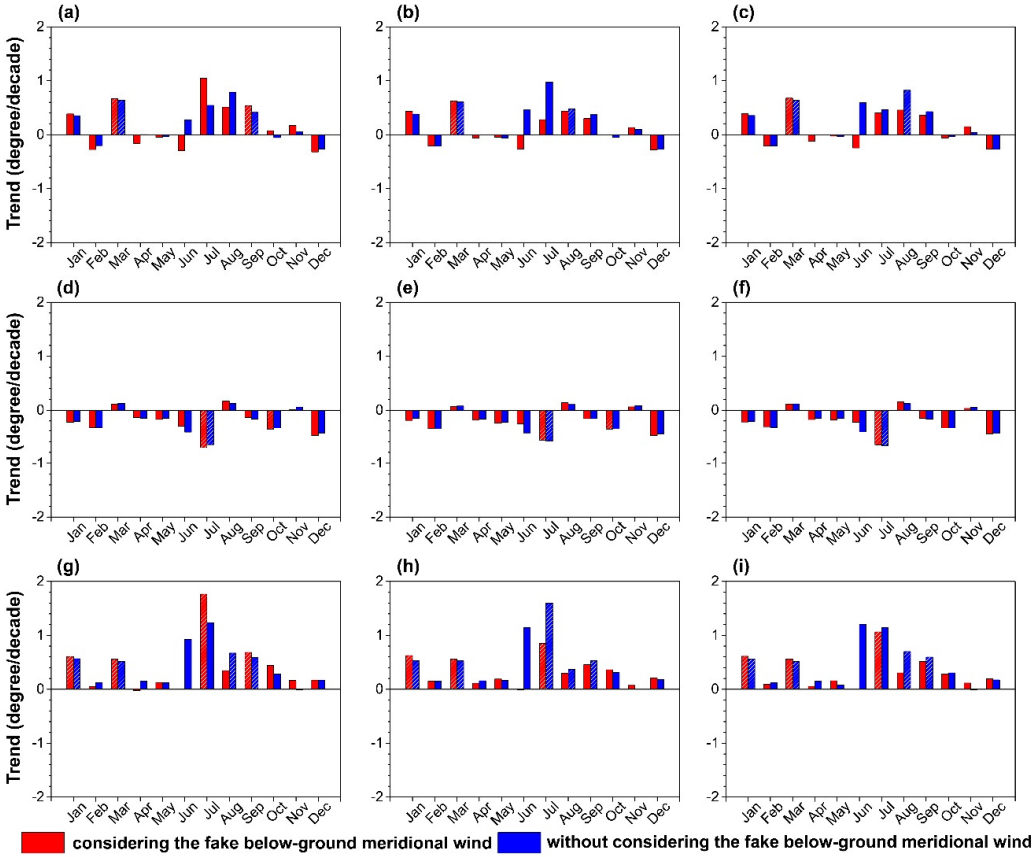

Figure 14. (**a**–**c**) Annual cycle of the linear trends of the NH HCW from 1979–2018 derived from (**a**) M1, (**b**) M2, and (**c**) M3 using the MRM data sets. The trends that passed the 95% statistical confidence level are filled with oblique lines. The red and blue bars are for the results that considered and did not consider FBGMW, respectively. (**d**–**f**) and (**g**–**i**) same as (**a**–**c**) but for the SH and TOT HCW, respectively. The units for the trends are degrees/decade.

4. Conclusions and Discussion

4.1. Conclusions

In this study, the impacts of FBGMW on HC in terms of the climatology, interannual variability, and long-term trends were investigated using five reanalysis data sets (i.e., the CFSR, ERA-Interim, ERA5, JRA-55, and NCEP2) based on three different computing methods (i.e., the traditional, 3P-DGAC, and local partitioning methods). The main conclusions obtained in this study do not rely on the choice of the reanalysis data. The following are the main conclusions of this study:

(1) The impacts of FBGMW on the climatology of the HCI were different based on the three methods, especially for the SH HCI. Specifically, not considering FBGMW led to underestimation of the NH HCI from January to May and October to December for M1, from January to June for M2, and from January to July and October to December for M3. In the SH, not considering FBGMW led to underestimation of the HCI in all months for M1 and from July to November for M3, while it had small effects in all months for M2;

(2) The impacts of FBGMW on the climatology of the rising and sinking branches and the width based on the three methods were similar, although some differences existed. Specifically, not considering FBGMW led to poleward shifts of the NE and CE during boreal summer and, thus, led to expansion of the NH HCW and TOT HCW and contraction of the SH HCW during boreal summer;

(3) The impacts of FBGMW on the interannual variability of the HC were similar based on the three methods. Specifically, FBGMW had a small impact on the NH HCI, CE, and SH HCW and had

an obvious impact on the NE, NH HCW, and TOT HCW from June to August, while it had nearly no impact on HC under other conditions;

(4) The impacts of FBGMW on the long-term trends of HC were similar based on the three methods. Specifically, FBGMW had an obvious impact on the NE, NH HCW, and TOT HCW from June to September and had a small impact on CE and SH HCW in June. Under other conditions, FBGMW had a very small impact on HC.

4.2. Discussion

The key finding of this study was that the FBGMW has vital influences on the NH HC during boreal summer. The previous analysis without considering FBGMW led to overestimation of the poleward expansion of the NH HC during boreal summer, and the long-term trends of the HC should be more accurately estimated after considering FBGMW. If FBGMW is considered, the poleward expansion of the NH HC in June is not visible. In July and September, it depends on the methods. In August, the poleward expansion of the NH HC is reduced. Thus, the previous studies related to the NH HC during boreal summer without considering FBGMW should be reconsidered.

It should be noted that although errors caused by not considering FBGMW exist in all months and hemispheres, only the NH HC during boreal summer has been greatly influenced. This is because the NH HC during boreal summer is very weak, the errors of the MSF caused by not considering FBGMW have more obvious influences on the NH HC during boreal summer than that in other months. This finding suggests that the FBGMW has larger influences during periods or at locations where the MSF is generally small. Thus, in future investigations, the FBGMW should be taken into consideration when or where the MSF is generally small.

Figures 15–17 display the global distribution of the FBGMW at 1000 hPa derived from M1, M2, and M3, respectively, using the MRM data sets. It can be found from Figures 15–17 that the FBGMW is quite different in different regions regardless of the method used, suggesting that the influences of FBGMW on the regional HC may be different in different regions and may be different from the global zonally averaged HC. Figures 15–17 also show that the FBGMW is different based on different methods in an exact month and region. Thus, the impact of FBGMW on the regional HC in different regions derived from the three methods should be further investigated in the future.

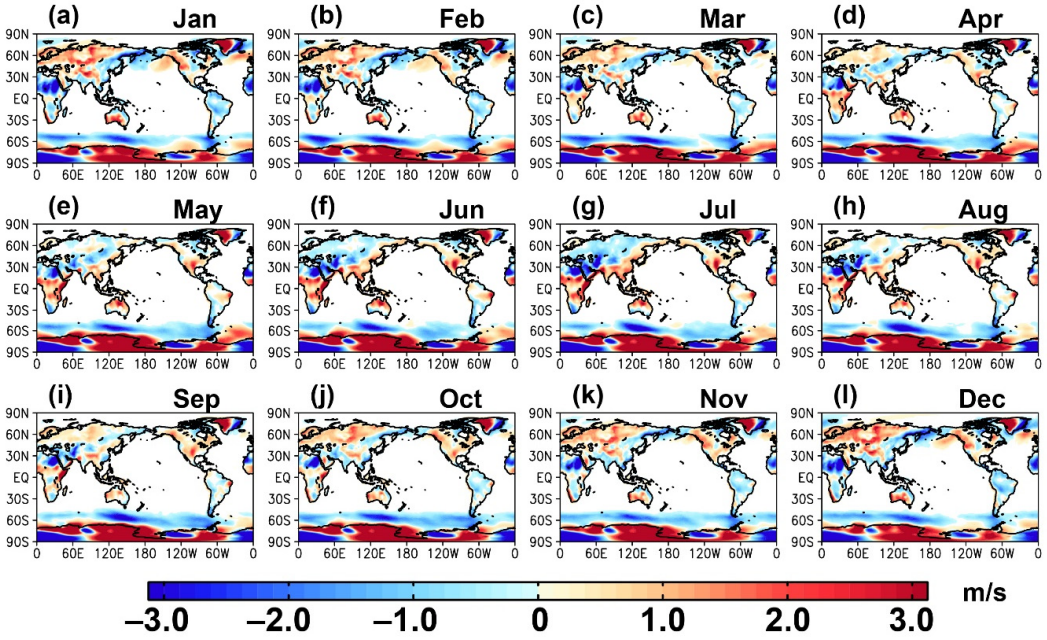

Figure 15. Global distribution of the FBGMW at 1000 hPa derived from M1 using the MRM data sets (1979–2018). (**a**–**l**) The FBGMW from January to December. The units for the FBGMW are m/s.

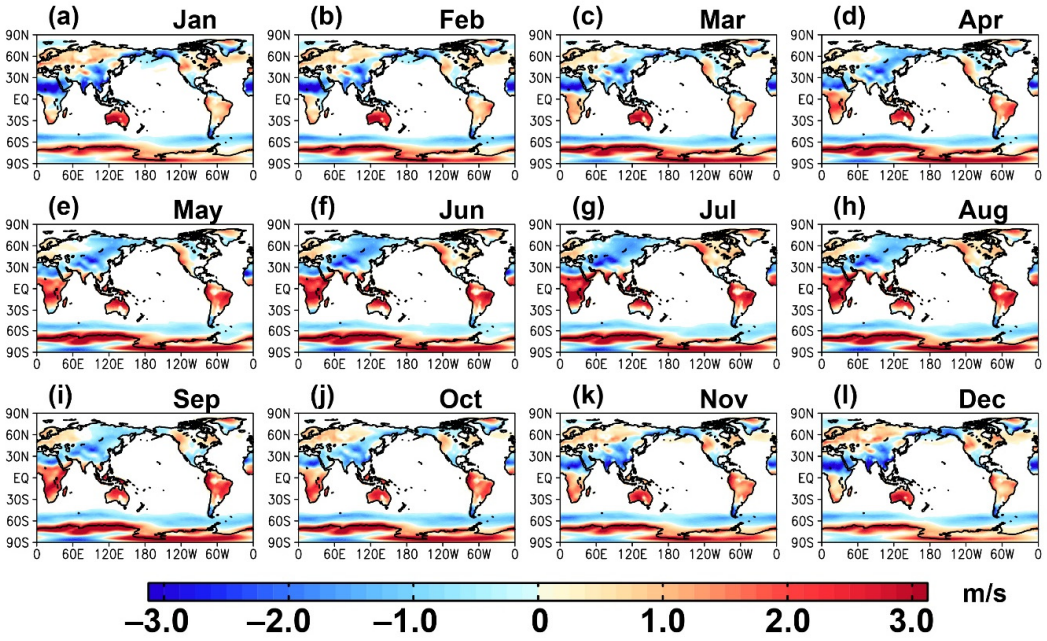

Figure 16. Same as Figure 15 but for the results derived from M2.

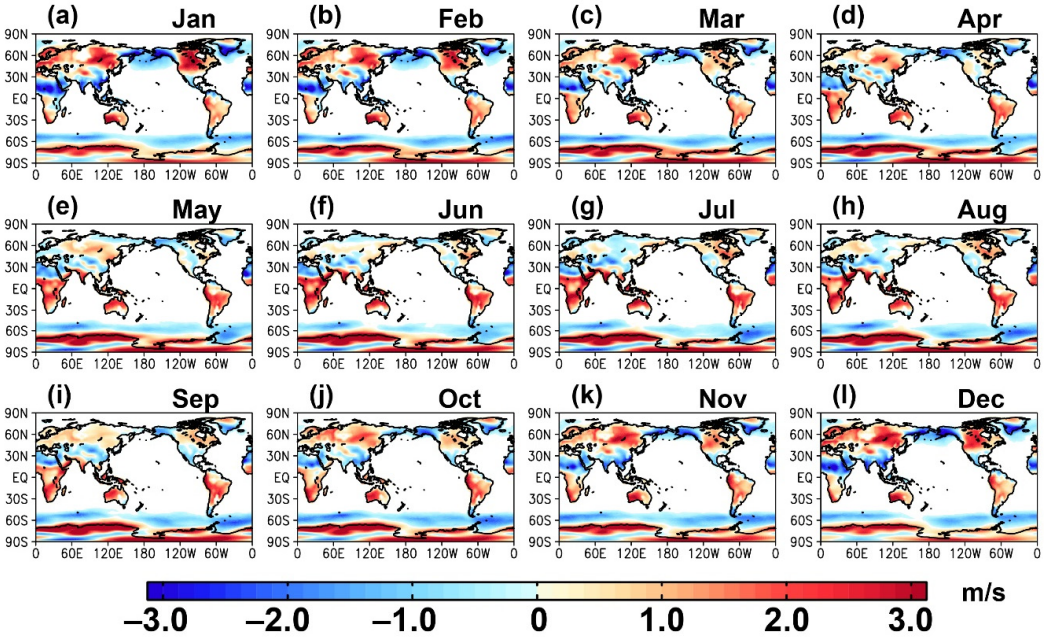

Figure 17. Same as Figure 15 but for the results derived from M3.

Supplementary Materials: The following are available online at http://www.mdpi.com/2073-4433/11/5/446/s1.

Author Contributions: Formal analysis, Z.X. and J.C.; Writing—Original draft, X.H. and J.C.; Writing—Review and editing, J.C. All authors have read and agreed to the published version of the manuscript.

Funding: This study was jointly supported by the National Key Research and Development Program of China (Grant 2017YFC1502305) and the National Natural Science Foundation of China (Grant 41775069).

Conflicts of Interest: The authors declare no conflict of interest.

References

1. Hadley, G. Concerning the cause of the general trade-winds. *Philos Trans.* **1735**, *39*, 58–62.
2. Bjerknes, J. A possible response of the atmospheric Hadley circulation to equatorial anomalies of ocean temperature. *Tellus* **1966**, *18*, 820–829. [CrossRef]
3. Oort, A.H.; Yienger, J.J. Observed interannual variability in the Hadley circulation and its connection to ENSO. *J. Clim.* **1996**, *9*, 2751–2767. [CrossRef]
4. Diaz, H.F.; Bradley, R.S. *The Hadley Circulation: Present, Past and Future*; Kluwer Academic Publishers: Dordrecht, The Netherlands, 2004.
5. Seidel, D.J.; Fu, Q.; Randel, W.J.; Reichler, T.J. Widening of the tropical belt in a changing climate. *Nat. Geosci.* **2008**, *1*, 21–24. [CrossRef]
6. Chen, J.; Carlson, B.E.; Del Genio, A.D. Evidence for strengthening of the tropical general circulation in the 1990s. *Science* **2002**, *295*, 838–841. [CrossRef] [PubMed]
7. Mitas, C.M.; Clement, A. Has the Hadley cell been strengthening in recent decades? *Geophys. Res. Lett.* **2005**, *32*, L03809. [CrossRef]
8. Sohn, B.; Park, S.C. Strengthened tropical circulations in past three decades inferred from water vapor transport. *J. Geophys. Res. Atmos.* **2010**, *115*, D15112. [CrossRef]
9. Liu, J.; Song, M.; Hu, Y.; Ren, X. Changes in the strength and width of the Hadley circulation since 1871. *Clim. Past.* **2012**, *8*, 1169–1175. [CrossRef]
10. Chen, S.; Wei, K.; Chen, W.; Song, L. Regional changes in the annual mean Hadley circulation in recent decades. *J. Geophys. Res. Atmos.* **2014**, *119*, 7815–7832. [CrossRef]
11. Wielicki, B.A.; Wong, T.; Allan, R.P.; Slingo, A.; Kiehl, J.T.; Soden, B.J.; Gordon, C.T.; Miller, A.J.; Yang, S.K.; Randall, D.A.; et al. Evidence for large decadal variability in the tropical mean radiative energy budget. *Science* **2002**, *295*, 841–844. [CrossRef]
12. Ma, J.; Li, J. Strengthening of the boreal winter Hadley circulation and its connection with ENSO. *Prog. Nat. Sci.* **2007**, *17*, 1327–1333.
13. Ma, J.; Li, J. The principal modes of variability of the boreal winter Hadley cell. *Geophys. Res. Lett.* **2008**, *35*, L01808.
14. Tanaka, H.L.; Ishizaki, N.; Kitoh, A. Trend and interannual variability of Walker, monsoon and Hadley circulations defined by velocity potential in the upper troposphere. *Tellus A* **2004**, *56*, 250–269. [CrossRef]
15. Mitas, C.M.; Clement, A. Recent behavior of the Hadley cell and tropical thermodynamics in climate models and reanalyses. *Geophys. Res. Lett.* **2006**, *33*, L01810. [CrossRef]
16. Freitas, A.C.V.; Aímola, L.; Ambrizzi, T.; de Oliveira, C.P. Changes in intensity of the regional Hadley cell in Indian Ocean and its impacts on surrounding regions. *Meteorol. Atmos. Phys.* **2017**, *129*, 229–246. [CrossRef]
17. Huang, R.; Chen, S.; Chen, W.; Hu, P.; Yu, B. Recent strengthening of the regional Hadley circulation over the western Pacific during boreal spring. *Adv. Atmos. Sci.* **2019**, *36*, 1251–1264. [CrossRef]
18. Staten, P.W.; Lu, J.; Grise, K.M.; Davis, S.M.; Birner, T. Re-examining tropical expansion. *Nat. Clim. Chang.* **2018**, *8*, 768–775. [CrossRef]
19. Hu, Y.; Fu, Q. Observed poleward expansion of the Hadley circulation since 1979. *Atmos. Chem. Phys.* **2007**, *7*, 5229–5236. [CrossRef]
20. Mathew, S.S.; Kumar, K.K.; Subrahmanyam, K.V. Hadley cell dynamics in Japanese Reanalysis-55 dataset: Evaluation using other reanalysis datasets and global radiosonde network observations. *Clim. Dyn.* **2016**, *12*, 3917–3930. [CrossRef]
21. Huang, R.; Chen, S.; Chen, W.; Hu, P. Interannual variability of regional Hadley circulation intensity over western Pacific during boreal winter and its climatic impact over Asia-Australia region. *J. Geophys. Res. Atmos.* **2018**, *123*, 344–366. [CrossRef]
22. Seidel, D.J.; Randel, W.J. Recent widening of the tropical belt: Evidence from tropopause observations. *J. Geophys. Res. Atmos.* **2007**, *112*, D20113. [CrossRef]
23. Lucas, C.; Nguyen, H.; Timbal, B. An observational analysis of Southern Hemisphere tropical expansion. *J. Geophys. Res. Atmos.* **2012**, *117*, D17112. [CrossRef]
24. Hudson, R.D.; Andrade, M.F.; Follette, M.B.; Frolov, A.D. The total ozone field separated into meteorological regimes—Part II: Northern Hemisphere mid-latitude total ozone trends. *Atmos. Chem. Phys.* **2006**, *6*, 5183–5191. [CrossRef]

25. Hu, Y.; Zhou, C.; Liu, J. Observational evidence for poleward expansion of the Hadley circulation. *Adv. Atmos. Sci.* **2011**, *28*, 33–44. [CrossRef]
26. Archer, C.L.; Caldeira, K. Historical trends in the jet streams. *Geophys. Res. Lett.* **2008**, *35*, L08803. [CrossRef]
27. Kang, S.M.; Polvani, L.M.; Fyfe, J.C.; Sigmond, M. Impact of polar ozone depletion on subtropical precipitation. *Science* **2011**, *332*, 951–954. [CrossRef]
28. Zhou, Y.P.; Xu, K.M.; Sud, Y.C.; Betts, A.K. Recent trends of the tropical hydrological cycle inferred from global precipitation climatology project and international satellite cloud climatology project data. *J. Geophys. Res. Atmos.* **2011**, *116*, D09101. [CrossRef]
29. Cheng, J.; Xu, Z.; Hu, P.; Hou, X.; Gao, C.; Hu, S.; Feng, G. Significant role of orography in shaping the northern Hadley circulation and its poleward expansion during boreal summer. *Geophys. Res. Lett.* **2018**, *45*, 6619–6627. [CrossRef]
30. Schwendike, J.; Govekar, P.; Reeder, M.J.; Wardle, R.; Berry, G.J.; Jakob, C. Local partitioning of the overturning circulation in the tropics and the connection to the Hadley and Walker circulations. *J. Geophys. Res. Atmos.* **2014**, *119*, 1322–1339. [CrossRef]
31. Schwendike, J.; Berry, G.J.; Reeder, M.J.; Jakob, C.; Govekar, P.; Wardle, R. Trends in the local Hadley and local Walker circulations. *J. Geophys. Res. Atmos.* **2015**, *120*, 7599–7618. [CrossRef]
32. Hu, S.; Cheng, J.; Chou, J. Novel three-pattern decomposition of global atmospheric circulation: Generalization of traditional two-dimensional decomposition. *Clim. Dyn.* **2017**, *49*, 3573–3586. [CrossRef]
33. Hu, S.; Chou, J.; Cheng, J. Three-pattern decomposition of global atmospheric circulation: Part I—Decomposition model and theorems. *Clim. Dyn.* **2018**, *50*, 2355–2368. [CrossRef]
34. Hu, S.; Cheng, J.; Xu, M.; Chou, J. Three-pattern decomposition of global atmospheric circulation: Part II—Dynamical equations of horizontal, meridional and zonal circulations. *Clim. Dyn.* **2018**, *50*, 2673–2686. [CrossRef]
35. Saha, S.; Moorthi, S.; Pan, H.L.; Wu, X.; Wang, J.; Nadiga, S.; Tripp, P.; Kistler, R.; Woollen, J.; Behringer, D.; et al. The NCEP Climate Forecast System Reanalysis. *Bull. Am. Meteorol. Soc.* **2010**, *91*, 1015–1057. [CrossRef]
36. Saha, S.; Moorthi, S.; Wu, X.; Wang, J.; Nadiga, S.; Tripp, P.; Behringer, D.; Hou, Y.T.; Chuang, H.Y.; Iredell, M.; et al. The NCEP Climate Forecast System Version 2. *J. Clim.* **2014**, *27*, 2185–2208. [CrossRef]
37. Dee, D.P.; Uppala, S.M.; Simmons, A.J.; Berrisford, P.P.; Kobayashi, S.; Andrae, U.; Balmaseda, M.A.; Balsamo, G.; Bauer, P.; Bechtold, P.; et al. The ERA-Interim reanalysis: Configuration and performance of the data assimilation system. *Q. J. R. Meteorol. Soc.* **2011**, *137*, 553–597. [CrossRef]
38. Hersbach, H.; Dee, D. ERA5 reanalysis is in production. *ECMWF Newsl.* **2016**, *147*, 7.
39. Kobayashi, S.; Ota, Y.; Harada, Y.; Ebita, A.; Moriya, M.; Onoda, H.; Onogi, K.; Kamahori, H.; Kobayashi, C.; Endo, H.; et al. The JRA-55 Reanalysis: General specifications and basic characteristics. *J. Meteorol. Soc. Jpn.* **2015**, *93*, 5–48. [CrossRef]
40. Kanamitsu, M.; Ebisuzaki, W.; Woollen, J.; Yang, S.K.; Hnilo, J.J.; Fiorino, M.; Potter, G.L. NCEP-DOE AMIP-II reanalysis (R-2). *Bull. Am. Meteorol. Soc.* **2002**, *83*, 1631–1643. [CrossRef]
41. Staten, P.W.; Grise, K.M.; Davis, S.M.; Karnauskas, K.; Davis, N. Regional widening of tropical overturning: Forced change, natural variability, and recent trends. *J. Geophys. Res. Atmos.* **2019**, *124*, 6104–6119. [CrossRef]